Research Square

Preprints are preliminary reports that have not undergone peer review.
They should not be considered conclusive, used to inform clinical practice,
or referenced by the media as validated information.

Deletion of a Distal IRF4 Element Prevents Inflammation-induced Reprogramming of Human Regulatory T-cell Fate

Qizhi Tang

Qizhi.Tang@ucsf.edu

University of California, San Francisco https://orcid.org/0000-0001-7313-3574

Patrick Ho

University of California, San Francisco https://orcid.org/0000-0003-4751-6904

Wendy Rosenthal

University of California, San Francisco

Jeffrey Bluestone

University of California, San Francisco

Article

Keywords:

Posted Date: November 7th, 2024

DOI: https://doi.org/10.21203/rs.3.rs-5356932/v1

License: This work is licensed under a Creative Commons Attribution 4.0 International License.
Read Full License

Additional Declarations: Yes there is potential Competing Interest. P.H. has no financial interests to report. P.H. is a coinventor of the following relevant pending patent: US Patent Application No. 63/571,413. W.R. has no conflict to report. Q.T. is a cofounder and shareholder of Sonoma Biotherapeutics, holds shares of stock in eGenesis, and is a scientific advisor for Sonoma Biotherapeutics, Qihan Bio, Minutia, Moderna, and Waypoint Bio. Q.T. is a coinventor of the following relevant issued patents and pending patents: US9801911B2, US7722862B2, PCT/US2019/022546, PCT/US2019/023883, PCT/US2020/030869, PCT/US2021/072139, PCT/US2021/049682, PCT/US2022/074720, and US Patent Application No. 63/571,413. J.A.B. is CEO and president and has a financial interest in Sonoma Biotherapeutics and is on the board of directors and has financial interests in Gilead. J.A.B. is a coinventor of the following relevant issued patents and pending patents:

PCT/US20230280341A1, PCT/US9801911B2, aU2016211161C1, PCT/US10138298B2, PCT/US7722862B2, PCT/US2019/022546, PCT/US2019/023883, PCT/US2021/072139, PCT/US2021/049682, and US Patent Application No. 63/571,413.

Version of Record: A version of this preprint was published at Nature Immunology on September 21st, 2026. See the published version at https://doi.org/10.1038/s41590-026-02655-8.

Deletion of a Distal *IRF4* Element Prevents Inflammation-induced Reprogramming of Human Regulatory T-cell Fate

Patrick Ho[1], Wendy Rosenthal[1], Jeffrey A. Bluestone[1], Qizhi Tang[1,2,3,*]
[1]Diabetes Center, University of California, San Francisco, San Francisco, CA 94143
[2]Department of Surgery, University of California, San Francisco, San Francisco, CA 94143
[3]Gladstone-UCSF Institute of Genomic Immunology, San Francisco, San Francisco, CA 94158

Abstract

Adoptive regulatory T cell (Treg) therapy is an emergent treatment paradigm for restoring immune tolerance in patients with autoimmune and inflammatory diseases. While preclinical models have demonstrated the remarkable efficacy of Treg cell therapy, lineage-tracing studies have also revealed that murine Tregs can lose lineage identity and adopt a proinflammatory state. Whether human Tregs exhibit a similar susceptibility to inflammatory cytokine-mediated lineage decommitment remains inconclusive. Here, we present an *in vitro* model of human Treg destabilization characterized by silencing of the Treg lineage-defining transcription factor, FOXP3, loss of suppressive activity, and gain of proinflammatory functions. Analysis of single-cell ATAC and transcriptomic profiles of Tregs during destabilization revealed a switch in chromatin accessibility between two elements at the *IRF4* locus. Excision of the distal *IRF4* element enabled Tregs to resist inflammatory cytokine-induced reprogramming, presenting a cell-engineering strategy to design more effective Treg therapies.

Regulatory T cells (Tregs) are a highly specialized subset of $CD4^+$ T cells characterized by constitutive FOXP3 expression and an ability to suppress the activities of other immune cells. Despite comprising a relatively small immunocyte fraction, Tregs play a dominant role in enabling peripheral immune tolerance through a myriad of mechanisms that collectively dampen antigen presentation, compete for T-cell growth factors, convert metabolites, promote tissue repair, and induce neighboring cells to develop tolerogenic activities[1,2]. Unsurprisingly, Treg dysfunction carries severe consequences, exemplified by the multi-organ autoimmunity manifest in immune dysregulation, polyendocrinopathy, enteropathy, X-linked (IPEX) syndrome, an often fatal monogenic disorder featuring *FOXP3* mutations that prevent terminal Treg differentiation[3–5]. Several groups have demonstrated that rescue of a functional, Foxp3-replete Treg compartment is sufficient to ameliorate the murine equivalent of IPEX in *scurfy* mice[3–5]. These findings have inspired novel therapeutic strategies aimed at boosting or harnessing Tregs to quell undesired immune responses without impeding protective immunity[6–8].

Adoptive Treg therapy is an emergent treatment paradigm in which *ex vivo*-expanded Tregs are administered as “living” drugs to promote tissue-specific immune tolerance in transplant and autoimmune disease patients[9–12]. The transfer of antigen-specific Tregs has shown remarkable efficacy across a broad array of preclinical models and is currently under clinical trial evaluation for numerous autoimmune disorders, including type 1 diabetes (T1D), rheumatoid arthritis (RA), multiple sclerosis (MS), and inflammatory bowel disease (IBD)[13]. However, lineage-tracing studies have also exposed a natural susceptibility for a subset of murine Tregs to downregulate Foxp3 and undergo epigenetic reprogramming following antigen encounter within chronically inflamed environments[14–16]. The resulting exFoxp3 cells show signs of destabilized Treg identity, with the consequent reduction in suppressive activity and acquisition of proinflammatory and/or cytotoxic functions ultimately fueling the capacity to mediate autoimmune tissue destruction[14–16]. This inflammation-induced lineage instability could hinder both the efficacy and safety of adoptive Treg therapy, as pathogenic conversion may not only compromise immunosuppressive functions, but also exacerbate transplant rejection or autoimmune disease progression.

Despite the potential ramifications for cell therapy applications, the molecular mechanisms underlying Treg destabilization in inflammatory settings are not well-understood. In humans, the lack of fate-mapping tools has made it difficult to conclusively identify cells that have transitioned from a Treg to exFOXP3 state. But recent studies have revealed overlaps between the T-cell receptor (TCR) repertoires of suppressive Tregs and clonally expanded, pathogenic effector-like cells from patients with chronic inflammatory diseases[16], providing evidence of either a shared progenitor or the conversion between cell states. Earlier reports have also highlighted differences in the stability and proliferative capacity of distinct FOXP3$^+$ subsets amongst CD4$^+$ T cells isolated from peripheral blood, including a population of CD4$^+$CD25$^+$CD45RA$^-$ cells with Th17 potential[17]. These cells are more prevalent in patients with active systemic lupus erythematosus (SLE) and are both functionally less suppressive and capable of secreting proinflammatory cytokines such as IL-17A[17]. When challenged with weekly cycles of *in vitro* TCR stimulation, these CD4$^+$CD25$^+$CD45RA$^-$ cells are also more prone to FOXP3 silencing[18].

But while FOXP3 activity is essential for Treg suppressive function, Treg identity also hinges on a unique epigenetic landscape marked by hundreds of differentially methylated regions (DMRs) that guide Treg-specific transcriptional programs[19–21]. For example, the Treg-exclusive absence of DNA methylation at the *FOXP3* conserved non-coding sequence (CNS)2 allows an embedded enhancer to drive constitutive FOXP3 expression. This aptly termed Treg-specific demethylated region (TSDR) is widely considered the most reliable indicator of Treg lineage-commitment[22]. Although the stepwise imprinting of Treg epigenetic signatures has been mapped in the context of thymic Treg development, regulation of the Treg epigenome in peripheral tissues remains poorly understood. In particular, several transcription factors have been reported to reinforce or undermine Treg identity[23–26], and the likely interplay between dysregulated gene regulatory networks and epigenetic rewiring in Treg fate decisions requires more thorough investigation.

Filling in these knowledge gaps could enable the design of Treg-based therapeutics with enhanced lineage stability, ensuring greater immunosuppressive efficacy and clinical safety. More broadly, the ability to manipulate Treg cell fates would also present opportunities to more effectively dampen or bolster immune responses in autoimmunity and cancer, respectively. Here, we present an *in vitro* model of inflammatory cytokine-driven human Treg instability, which enabled the capture of molecular profiles in primary human Tregs actively undergoing destabilization and development of a cell engineering strategy to stabilize Treg identity and preserve suppressive function.

Results

Prolonged *in vitro* inflammatory cytokine exposure induces human Treg instability and dysfunction

To investigate whether human Tregs are susceptible to losing lineage identity, CD4$^+$CD25$^+$CD127$^{lo/-}$ FACS-isolated primary human Tregs were subjected to repeated 9-day cycles of *in vitro* CD3/CD28 stimulation in the presence or absence of high levels of proinflammatory cytokines (Fig. 1a). As a preliminary gauge of Treg identity, we focused on FOXP3 and HELIOS, a key pair of transcription factors (TFs) with well-established, complementary roles in regulating Treg fitness and suppressive function[27–30]. Since human conventional CD4$^+$ T cells (Tconvs) transiently express FOXP3 following TCR activation, expression profiles were evaluated 7 days into each stimulation cycle, after FOXP3 protein levels had mostly waned in non-Tregs. Under prolonged inflammatory cytokine exposure, primary human Tregs progressively downregulated both FOXP3 and HELIOS, resulting in the emergence of a FOXP3$^-$HELIOS$^-$ population (Fig. 1b). Since Tconvs rapidly out-proliferate Tregs *in vitro*, an expansion of FOXP3$^-$HELIOS$^-$ cells could also indicate imperfect Treg purity

during the initial Treg isolation. However, the absence of FOXP3^{-}HELIOS^{-} cells in parallel cultures without inflammatory cytokines signified high initial Treg purity (Fig. 1b) and supported an inflammatory cytokine-dependent effect.

The gradual loss of FOXP3 and HELIOS expression over the culture period was observed following exposure to different inflammatory cytokines or cytokine combinations associated with distinct helper T-cell (Th) subsets, including Th1 (IL-12), Th2 (IL-4), and Th17 (IL-6, IL-1β, IL-23) (Extended Data Fig. 1). Since the Th17-promoting combination of IL-6, IL-1β, and IL-23 appeared most effective at inducing FOXP3 and HELIOS silencing (Extended Data Fig. 1), this triple combination was selected for more in-depth characterization. The extent of Treg destabilization was dependent on both the level and duration of inflammatory exposure. The fraction of FOXP3^{-}HELIOS^{-} cells scaled with the concentration of exogenously added IL-6, IL-1β, and IL-23 across a 50-fold range (Fig. 1c). Moreover, transient exposure to the inflammatory cytokines for 7 days during the first cycle of stimulation was sufficient to drive the loss of FOXP3 and HELIOS in subsequent cycles, albeit in a smaller proportion of cells than under conditions of persistent cytokine exposure (Extended Data Fig. 2). Abrogating the inflammatory cytokine exposure reduced FOXP3^{-}HELIOS^{-} cell conversion, but the destabilized cells did not revert to a HELIOS^{+} state, suggesting a more permanent change in cell identity.

To determine if the loss of FOXP3 and HELIOS expression reflected an epigenetically delineated change in Treg fate, the HELIOS^{+}, FOXP3^{+}HELIOS^{-}, and FOXP3^{-}HELIOS^{-} populations were FACS-purified and evaluated for the degree of DNA demethylation at the TSDR (Fig. 1d). This evolutionarily conserved *FOXP3* enhancer region features a stretch of CpG sites that is uniquely devoid of methylation in Tregs but is completely methylated in Tconvs and other non-Tregs[31,32]. The TSDR was predominantly demethylated in HELIOS^{+} cells, consistent with a highly stable, committed Treg population. Meanwhile, FOXP3^{-}HELIOS^{-} cells exhibited substantial TSDR methylation, consistent with destabilization of the Treg epigenome. The degree of TSDR methylation in FOXP3^{-}HELIOS^{-} cells was not complete, which could also result from a mixed population of demethylated Tregs and methylated non-Tregs. However, rather than a uniform methylation profile across the TSDR, individual CpG sites were re-methylated to different levels (Extended Data Fig. 3), indicating the presence of cells undergoing a transition in cell state and providing additional evidence that this population did not expand from TSDR-methylated Tconvs. Together, these data showed that patterns of HELIOS^{+} or FOXP3^{-}HELIOS^{-} expression could serve as an accurate proxy for committed or destabilized Treg identity, respectively.

Single-cell profiles reveal transcriptomic and epigenetic hallmarks of Treg destabilization

Having shown that the Treg epigenome could be destabilized by repeated TCR stimulation in the presence of IL-6, IL-1β, and IL-23 exposure, we sought to determine whether the function of *in vitro* destabilized Tregs was affected. Tregs treated with IL-6, IL-1β, and IL-23 progressively downregulated the IL-2 receptor α chain (CD25), CTLA-4, ICOS, and TIGIT (Fig. 2a, Extended Data Fig. 4a), consistent with a less suppressive phenotype relative to Tregs expanded in the standard IL-2–only conditions. Conversely, IL-6, IL-1β, and IL-23-exposed cells upregulated CD226 and CD40LG (Fig. 2A, Extended Data Fig. 4a), markers that have been implicated in Treg dysfunction[33,34]. Co-culture assays with peripheral blood mononuclear cells (PBMCs) showed a reduction in the *in vitro* suppressive activity of inflammatory cytokine-exposed Tregs (Fig. 2b). Treg dysfunction also coincided with increased cell expansion (Fig. 2c) and IFNγ, TNFα, and IL-17A production (Fig. 2d, Extended Data Fig. 4b), highlighting the potential of these Tregs to acquire proinflammatory functions. Collectively, these data demonstrate that human Treg can lose lineage identity and become dysfunctional during repeated *in vitro* TCR stimulation in the presence of inflammatory cytokines.

Equipped with a robust model of human Treg destabilization, we next set out to elucidate molecular hallmarks and key regulators of Treg instability. Multi-omic single-cell transcriptional

and chromatin accessibility profiles were generated from the nuclei of primary human Tregs actively undergoing destabilization following 16 and 25 days of IL-6, IL-1β, and IL-23 exposure. Donor-matched Tregs from IL-2–only cultures and Tconvs were also profiled to serve as reference samples. Ten clusters were identified on a weighted nearest-neighbor (WNN) UMAP that accounts for both sequenced modalities (Fig. 3a). While there was little change in the cluster distribution between Day 16 and Day 25 for samples maintained in IL-2 alone, the IL-6, IL-1β, and IL-23 exposure drove a subset of cells toward a progressively Tconv-like state (Fig. 3b). Inspection of cluster-defining transcriptional features revealed that the resting Treg (rest Tr), effector Treg (eff Tr), and TNFR2-hi Treg (TNFR2hi Tr) clusters shared high expression of stable Treg markers, including FOXP3, IKZF2 (encoding HELIOS), CD27, CD25, CTLA-4, ICOS, and TIGIT (Fig. 3c). Conversely, the cycling Treg (cyc Treg), cytotoxic Treg (cytox Tr), and inflammatory Treg (infl Tr) clusters all exhibited transcriptional profiles consistent with a loss of Treg lineage identity, with downregulation of FOXP3 and HELIOS and upregulation of proinflammatory cytokine and/or cytotoxicity genes, such as IFNγ, TNFα, and IL-17A, or NKG7, GZMB, GZMA, and PFN1, respectively (Fig. 3c). We will collectively refer to cells in these clusters as destabilized or putative (ex)Tregs hereafter.

Many of these differences in gene expression correlated with altered chromatin accessibility at the encoding locus. For example, downregulation of FOXP3 transcription in the destabilized Treg clusters matched a loss of chromatin accessibility at the *FOXP3* CNS2 enhancer region, which encompasses the TSDR (Fig. 3d). The opposite was observed for IFNγ and GZMB, as increased chromatin accessibility at each respective locus was linked to transcriptional upregulation in the destabilized Treg clusters (Fig. 3d). These specific examples of epigenetic reprogramming mirrored a broader pattern of distinct open chromatin regions (OCRs) in destabilized Tregs, with a pronounced reduction in chromatin accessibility at stable Treg OCRs as well as acquisition of OCRs normally inaccessible in stable Tregs (Fig. 3e). Many of these changes overlapped differences in chromatin accessibility that distinguish Tconvs from Tregs, but a subset of OCRs appeared unique to destabilized Tregs (Fig. 3f), suggesting that destabilized Tregs are still epigenetically distinct from Tconvs. Together with the absence of cells in the destabilized Treg and Tconv clusters that originated from IL-2–only Treg samples, these findings further highlight that the emergence of FOXP3^{+}HELIOS^{-} cells was highly unlikely to be due to outgrowth of a pre-existing T effector cell population.

Destabilized Tregs are characterized by a chromatin accessibility switch at the *IRF4* locus

Although IL-6, IL-1β, and IL-23 exposure led to a sizeable number of destabilized cells, a substantial fraction retained strong commitment to Treg identity (Fig. 4a). To identify putative drivers of these distinct Treg fates, we analyzed the OCRs from stable and destabilized Tregs for differential TF motif enrichment. Destabilized Tregs showed a relative depletion of FOXP3 and E-box motifs along with enrichment of AP-1, ETS, and IRF4 motifs (Fig. 4b). In Tregs, IRF4 is essential for the full range of Treg-mediated immunosuppression, evidenced by the spontaneous development of Th2-mediated autoimmunity in Treg-specific IRF4 knockout (KO) mice[35]. Intriguingly, the AP-1 and ETS TF families both have numerous well-characterized members that heterodimerize with IRF4 and influence the binding site selectivity of the resulting TF complex. For example, BATF directs IRF4 to bind AP-1–IRF composite elements (AICEs), while PU.1 guides IRF4 to bind ETS–IRF composite elements (EICEs)[36]. Aside from regulating suppressive activities in mature Tregs, IRF4 also plays a central role in T-helper differentiation, in which TCR signaling fine-tunes IRF4 abundance to control T-helper cell fate[37,38].

Inspection of the *IRF4* locus revealed a gradual loss of chromatin accessibility at a TF motif-rich proximal OCR (OCR_{prox}) located within intron 6 (Fig. 4c, Extended Data Fig. 5). In Tregs, IRF4 expression has been reported to be FOXP3-dependent[35], and OCR_{prox} contains a FOXP3 binding site that has been previously identified in FOXP3 ChIP-seq experiments with

both mouse and human Tregs[39]. The loss in OCR_{prox} chromatin accessibility was accompanied by a reciprocal gain in chromatin accessibility at a distal OCR (OCR_{dist}) located +40 kb downstream of the IRF4 transcriptional start site (Fig. 4c). Peak-gene linkage analysis revealed that chromatin accessibility at OCR_{dist} was positively correlated with IRF4 transcript counts, hinting at potential enhancer activity and a putative enhancer switch as Tregs transitioned from a stable to destabilized state.

IRF4 OCR_{dist} selectively supports IRF4 expression in destabilized Tregs

Since IRF4 expression is upregulated in response to TCR signaling, the relatively low number of IRF4 transcripts detected in the multiome dataset may have been due to sampling at a time point after maximal IRF4 expression had already subsided. Therefore, IRF4 expression was tracked over the course of IL-6, IL-1β, and IL-23-induced instability to assess IRF4 expression kinetics. IRF4 upregulation was transient in both Tregs and Tconvs, peaking on day 2 and declining by day 5 of each anti-CD3/CD28 stimulation cycle (Fig. 5a, 5b). Peak IRF4 expression was higher in Tconvs than in Tregs. Moreover, destabilized $FOXP3^{-}HELIOS^{-}$ cells exhibited higher peak IRF4 expression than stable $HELIOS^{+}$ Tregs, indicating dysregulation of IRF4 expression (Fig. 5c, 5d). To investigate the impact of OCR_{prox} and OCR_{dist} on IRF4 expression, paired single-guide RNAs (sgRNAs) flanking each OCR were designed to enable CRISPR/Cas9-mediated excision from primary human Tregs prior to inducing destabilization (Extended Data Fig. 6a, 6b). As a mock CRISPR-editing control, the AAVS1 safe harbor locus was also targeted. Neither deletion of OCR_{prox} nor OCR_{dist} significantly altered IRF4 expression in cells that retained HELIOS expression (Fig. 5e, 5f). However, IRF4 induction was significantly reduced in $FOXP3^{-}HELIOS^{-}$ cells following OCR_{dist} removal (Fig. 5e, 5f), suggesting that OCR_{dist} selectively supported elevated IRF4 expression in Tregs that have become destabilized.

CRISPR-mediated *IRF4* OCR_{dist} excision prevents inflammatory cytokine-mediated Treg destabilization

Despite not having a significant effect on IRF4 expression, excision of OCR_{prox} mildly exacerbated IL-6, IL-1β, and IL-23-induced Treg destabilization (Fig. 6a), leading to a 30% increase in $FOXP3^{-}HELIOS^{-}$ cells by Day 25 relative to donor-matched AAVS1-edited controls (Fig. 6b). This suggests that OCR_{prox} has a protective role in maintaining Treg identity, although this regulation appears to occur through an indirect mechanism rather than by acting as a direct IRF4 enhancer. Meanwhile, ΔOCR_{dist} Tregs retained a remarkably high degree of lineage-stability (Fig. 6a), with an 85% reduction in the proportion of $FOXP3^{-}HELIOS^{-}$ cells over the course of prolonged inflammatory cytokine exposure when compared to donor-matched AAVS1-edited controls (Fig. 6b). This observed improvement in Treg stability could be achieved either by preventing the destabilization of stable $HELIOS^{+}$ Tregs or by hindering the expansion of destabilized exTregs that have lost FOXP3. Comparison of ΔOCR_{dist} Tregs to AAVS1-edited counterparts under destabilizing culture conditions revealed that OCR_{dist} excision resulted in elevated FOXP3 MFI in stable $HELIOS^{+}$ Tregs (Fig. 6c, 6d). Moreover, while the majority of cycling ($KI\text{-}67^{+}$) cells were $FOXP3^{-}$ in AAVS1-edited or ΔOCR_{prox} cultures, most proliferating ΔOCR_{dist} Tregs retained FOXP3 expression (Fig. 6e, 6f). Thus, both increased Treg stability and decreased exTreg fitness may contribute to the overall resistance against destabilization observed over the course of *in vitro* inflammatory cytokine exposure.

IRF4 ΔOCR_{dist} Tregs mediate greater protection from xenogeneic GvHD

The marked preservation of Treg identity by OCR_{dist} deletion has the potential to enhance both the clinical safety and efficacy of engineered Treg therapies. Unlike AAVS1-edited Tregs, which downregulated CD25, CTLA-4, ICOS, and TIGIT over the course of sustained IL-6, IL-1β, and IL-23 exposure, ΔOCR_{dist} Tregs maintained a suppressive phenotype (Extended Data Fig. 7). Accordingly, ΔOCR_{dist} Tregs were more effective than AAVS1-edited Tregs at

suppressing the proliferation of responder $CD4^+$ and $CD8^+$ T cells when co-cultured with dye-labeled PBMCs (Fig. 7a). To determine whether the superior *in vitro* suppressive activity of ΔOCR_{dist} Tregs would translate to enhanced *in vivo* function, we adapted an established model for Treg-mediated prevention of xenogeneic graft-versus-host disease (GvHD), in which *ex vivo*-expanded Tregs and donor-matched PBMCs are co-injected into NOD.Cg-$Prkdc^{scid}$ $Il2rg^{tm1Wjl}$/SzJ (NSG) mice.

Since the myeloid cells primarily responsible for producing IL-6, IL-1β, and IL-23 are known to engraft poorly in NSG mice, we pre-sensitized AAVS1-edited and ΔOCR_{dist} Tregs with 16 days of *in vitro* inflammatory cytokine exposure prior to cell injection (Fig. 7b). This pre-treatment was designed to force Tregs to the threshold of destabilization, thereby enabling a more accurate assessment of the functional impairment induced by Treg instability. To gauge the activity of non-sensitized Tregs, a group of AAVS1-edited Tregs was also expanded in the absence of IL-6, IL-1β, and IL-23 exposure (Fig. 7b). Following co-injection, mice were weighed twice weekly while being monitored for signs of GvHD in a blinded fashion until meeting humane endpoint necessitating euthanasia (weight loss exceeding 15% or predefined body score). All 3 groups of Tregs significantly prolonged mouse survival compared to the PBMC only (no Tregs) control group, indicating that even Tregs that had been pre-sensitized to inflammatory cytokine-driven instability still retained some suppressive activity (Fig. 7c). Interestingly, ΔOCR_{dist} Tregs were able to further enhance mouse survival relative to AAVS1-edited Tregs that had not been pre-challenged with IL-6, IL-1β, and IL-23, granting greater protection despite having undergone inflammatory cytokine exposure prior to injection. Collectively, these results demonstrate that engineered ΔOCR_{dist} Tregs acquire greater resistance to inflammatory cytokine-induced destabilization as well as increased suppressive potency *in vitro* and *in vivo*, presenting a strategy for generating safer and stronger adoptive Treg therapies.

Discussion

In this study, we developed an *in vitro* culturing system that promoted human Treg destabilization through repeated CD3/CD28 stimulation in the presence of inflammatory cytokine. Under normal *in vitro* expansion conditions with IL-2 alone, $CD4^+CD25^+CD127^{lo/-}$ FACS-purified primary human Tregs maintained high expression of FOXP3, HELIOS, and other Treg-defining markers, demonstrating an extraordinary degree of lineage stability in the absence of proinflammatory signals. In contrast, the addition of exogenous inflammatory cytokines during repetitive *in vitro* stimulation caused human Tregs to progressively downregulate FOXP3 and HELIOS expression, acquire TSDR re-methylation, and lose *in vitro* suppressive activity. Unlike lineage-stable Tregs, which co-express FOXP3 and T-helper programs to facilitate more specialized trafficking and suppression[40], the *in vitro* destabilized Tregs lost FOXP3 expression and did not revert to a stable Treg state even after prolonged recovery in IL-2 alone. Both the dose and duration of inflammatory cytokine exposure influenced the degree of Treg destabilization. Combined with the epigenetic conversion toward a mostly methylated TSDR, these results demonstrate that human Tregs can lose lineage identity and function during repeated antigen stimulation under prolonged inflammatory cytokine exposure. It is important to note that this *in vitro* model of Treg instability that may not fully replicate the complexity of signals that Tregs encounter in chronically inflamed tissues. Whether human Tregs naturally undergo destabilization and contribute to chronic inflammation within patients has yet to be conclusively demonstrated and remains difficult to study. The molecular signatures of human Treg lineage-decommitment identified in this study may aid future investigations.

The robust *in vitro* generation of destabilized human Tregs enabled us to investigate the molecular programs that contribute to Treg lineage-decommitment. Toward this goal, we generated single-cell multi-omic profiles of chromatin accessibility and gene expression, which revealed a striking dichotomy in the apparent usage of two non-coding regions at the *IRF4* locus. Neither OCR_{prox} nor OCR_{dist} have been previously reported to regulate IRF4 expression or

Treg identity. Deletion of OCR_{prox} mildly exacerbated Treg instability but had little effect on IRF4 expression. Meanwhile, removal of OCR_{dist} selectively prevented the increase of IRF4 expression in destabilized cells and maintained high expression of FOXP3, especially in proliferating Tregs. Thus, OCR_{dist} appears to selectively support the survival and/or proliferation of cells that have downregulated FOXP3, and the overall enhancement in Treg stability mediated by OCR_{dist} deletion may be due to an imposed selective pressure to maintain FOXP3 expression. Future work will be required to fully elucidate how potential counterregulatory interactions between OCR_{prox} and OCR_{dist} modulate Treg identity and function.

While the precise mechanisms linking these *IRF4* OCRs to Treg stability have yet to be fully deciphered, IRF4 is a well-established mediator of effector Treg programs, and is directly regulated by FOXP3 both transcriptionally and via protein-protein interaction[35]. Interestingly, IRF4 also plays a deterministic role in the differentiation of naïve Tconvs into other T-helper subsets[37]. Thus, IRF4 supports effector Treg programs under the direction of FOXP3, but naturally promotes alternative helper T-cell fates in the absence of FOXP3. There is also evidence that IRF4 itself can influence FOXP3 expression. Multiple groups have reported elevated numbers of $Foxp3^+$ Tregs in $Irf4^{-/-}$ mice, and $Irf4^{-/-}$ naïve Tconvs more readily differentiate into $Foxp3^+$ Tregs *in vitro*[35,41]. A recent study showed that Irf4-Batf3 complexes can coordinately interfere with the Foxp3 super enhancer to enforce Foxp3 repression and dissuade murine Treg differentiation *in vitro*[42]. Furthermore, IRF4 has been reported to participate in pioneering activity, often in conjunction with AP-1 family members[43]. Therefore, aberrant IRF4 activity may supersede FOXP3 control to participate in driving broader epigenetic rewiring that ultimately unravels Treg lineage identity. Future studies will be necessary to fully elucidate the role of IRF4 in human Treg destabilization.

Given that IRF4 has been reported to both dampen FOXP3 expression and promote key Treg activities, its net impact on Treg stability and function is likely to hinge on its association with other transcription factors. The real-time distribution of IRF4 amongst its potential complexes can be influenced by differences in the relative expression levels of either IRF4 or its binding partners. Since the gain of OCR_{dist} accessibility coincides with the IRF4 upregulation observed in destabilized cells, one potential mechanism is that excessive IRF4 expression oversaturates the pool of transcription factor complexes that can be controlled by FOXP3 and other Treg-promoting TFs. Alternatively, the switch from OCR_{prox} to OCR_{dist} may enable a different set of IRF4-interacting TFs to selectively promote IRF4 expression only when those TFs are available to partner with IRF4. This mode of epigenetic reprogramming is more commonly observed during cell development. For example, an enhancer switching event at the murine Irf8 locus from an E-box–dependent enhancer to a Batf3-dependent enhancer facilitates conventional dendritic cell type 1 (cDC1) development from progenitor DC cells by coupling Irf8 expression to Batf3 expression[44]. It is possible that OCR_{prox} couples IRF4 expression with FOXP3 expression to ensure FOXP3-mediated regulation over IRF4 binding, while the switch to OCR_{dist} simply allows aberrant IRF4 expression in the absence of FOXP3. It remains to be seen whether OCR_{prox} and OCR_{dist} restrict IRF4 expression to be dependent on specific TFs that drive opposing Treg fates.

Despite long-standing evidence that a Treg-specific epigenetic landscape is required for the stabilization of Treg identity and function[19,21,31,45], the regulatory networks that shape and maintain the Treg epigenome remain poorly defined. In this study, we identified *IRF4* non-coding regions that promote opposing Treg fates, underscoring the untapped potential in targeting the epigenetic interactions that underpin cell identity. Beyond uncovering OCR_{prox} and OCR_{dist} as a novel regulatory module, we spotlight the genetic disruption of OCR_{dist} as a strategy that can be incorporated into the design of engineered Treg therapies to ensure greater safety and suppressive potency. The *in vitro* model of human Treg destabilization introduced in this study also lays the groundwork for future studies to identify additional regulatory nodes and deepen

our understanding of the TF networks coordinating the preservation or dismantlement of Treg identity.

Methods

Treg Isolation

Peripheral blood mononuclear cells (PBMCs) from de-identified, healthy human donors were commercially obtained through Stemcell Technologies. $CD4^+$ T cells were negatively selected via the EasySep Human $CD4^+$ T-cell Enrichment Cocktail (Stemcell Technologies). $CD4^+CD25^+CD127^{lo/-}$ Tregs and $CD4^+CD25^-CD127^+$ Tconvs were subsequently isolated via FACS using FACSAria II or FACSAria III (Becton Dickinson) cell sorters to > 98% purity. Isolated cells were washed with culture media and plated at 1 x 10^6 cells/mL.

Cell Culture

Freshly isolated primary human Tregs and Tconvs were stimulated every 9 days with either CD3/CD28 Dynabeads (ThermoFisher Scientific) at 1:1 cell:bead ratio or with CD3/CD28/CD2 Immunocult (Stemcell Technologies) at 25 µL/mL. Cultures were maintained in RPMI-1640 (Gibco) supplemented with 10% heat-inactivated fetal bovine serum (FBS), 1% penicillin-streptavidin (Gibco), 1% MEM non-essential amino acids (Gibco), 10 mM HEPES (Gibco), and 1 mM sodium pyruvate (Gibco). Recombinant human IL-2 (Roche) was supplied at 300 IU/mL IL-2 during the initial 9-day stimulation cycle and 100 IU/mL IL-2 thereafter. For *in vitro* Treg destabilization, recombinant human cytokines were used at the following concentrations unless otherwise indicated: 25 ng/mL IL-6 (Peprotech), 20 ng/mL IL-1β (Peprotech), 20 ng/mL IL-23 (Peprotech), 20 ng/mL IL-12 (Peprotech), and/or 10 ng/mL IL-4 (Peprotech).

Genome Editing

CRISPR/Cas9 ribonucleoprotein (RNP) complexes were prepared by co-incubating chemically modified CRISPR sgRNAs (Synthego) and purified recombinant Cas9-NLS protein (UC Berkeley QB3 Macrolab) at 1:1 molar ratio. 1 x 10^6 Tregs or Tconvs were electroporated with 20 µM pre-complexed RNPs 64h after initial CD3/CD28 stimulation using program EO-115 on a Nucleofector 4D (Lonza). For excision edits with paired sgRNAs, 20 µM of each pre-complexed RNP was co-delivered simultaneously. At 4 days following CRISPR/Cas9 RNP delivery, genomic DNA was harvested from the edited cells for PCR amplification of the target loci and subsequent assessment of editing efficiency.

Guide RNA sequences used for the following edits:
AAVS1: GGGCCACUAGGGACAGGAU
IRF4 OCR_{prox}: UAUAGUAGGUAAGAUCUCCA and GCUCCUCAGCCAGACCGCAG
IRF4 OCR_{dist}: CCACUGGGAAACAAACCUGC and UACGUUGGAUCCCAUCACCC

Flow Cytometry

Cells were harvested at the indicated time points and stained for flow cytometry. For intracellular staining, cells were fixed and permeabilized with the Foxp3 Transcription Factor Staining Buffer Set (eBioscience). For intracellular cytokine staining, cells were treated with 0.5 µg/mL PMA (Abcam), 1 µg/mL Ionomycin (Sigma), and Brefeldin A (ThermoFisher) for 5h before staining. Data were collected on Fortessa flow cytometers (Becton Dickinson) or Aurora spectral flow cytometers (Cytek) and analyzed via FlowJo software (TreeStar).

TSDR Bisulfite Sequencing

$HELIOS^+$, $FOXP3^+HELIOS^-$, and $FOXP3^-HELIOS^-$ cells were isolated from *in vitro* destabilization cultures via FACS, washed, pelleted, and frozen at -80ºC. Cell pellets were submitted to EpigenDX according to vendor instructions for genomic DNA isolation, bisulfite conversion, and targeted pyrosequencing of the human FOXP3 TSDR (EpigenDX assay #ADS783-FS2).

In Vitro Suppression Assay

Cryopreserved PBMCs were thawed and labeled with CellTraceViolet (ThermoFisher) according to manufacturer instructions. For *in vitro* suppression assays, 7.5 x 10^4 CTV-labeled responder PBMCs were co-cultured with expanded Tregs at the indicated PBMC:Treg ratios and stimulated with 1 µg/mL soluble anti-CD3 (clone Hit3a, BD Biosciences) and 0.5 µg/mL soluble anti-CD28 (clone 28.2, Biolegend) for 3 days. Cultures were then harvested and stained with Fixable Live/Dead Viability Dye eFluor780 (ThermoFisher), CD4_PE (clone RPA-T4, BD Biosciences), CD8A_FITC (clone SK1, BD Biosciences), and CD25_APC (clone 2A3, BD Biosciences) prior to flow cytometry and assessment of responder PBMC proliferation.

Xenogeneic Graft-vs.-Host Disease Model

NOD.Cg-Prkdc^{scid} Il2rg^{tm1Wjl}/SzJ (NSG) mice were obtained from Jackson Laboratories. For GvHD induction, animals were irradiated (1.75 Gy) 24h prior to retro-orbital intravenous (i.v.) injection of 4 x 10^6 PBMCs with 4 x 10^6 *in vitro*-expanded, PBMC-matched Tregs. Mice were monitored and weighed twice weekly by researchers who were blinded to the treatment conditions. Mice were euthanized upon reaching pre-defined humane endpoint of exhibiting >15% weight loss or worsening body conditions. All mouse experiments were performed according to a UCSF Institutional Animal Care and Use Program (IACUP)-approved protocol (IACUC protocol no. AN200668).

Single-cell Multiome (ATAC + Gene Expression) Sequencing

Nuclei were isolated from *in vitro*-expanded Tregs and Tconvs at the indicated time points prior to preparation of single-cell multiome sequencing libraries with the Chromium Next GEM Single Cell Multiome ATAC + Gene Expression kit (10X Genomics), according to manufacturer instructions. Sequencing was performed on a NovaSeq 6000 (Illumina) and data were processed with Bcl2fastq and Cell Ranger ARC 2.02 (10X Genomics). Data were subsequently analyzed using Seurat[46] v4 and Signac[47] v1.10.

Single-cell Data Pre-processing

The SoupX[48] package was used to estimate and remove ambient RNA contamination in each sample. Low-quality cells and multiplets were subsequently filtered by removing outliers in the transcriptomic data for total transcript counts, number of distinct features, and fraction of transcripts mapping to mitochondrial genes. Similarly, outliers in the ATAC data were removed by examining total fragment counts, number of distinct features, and ratio of mononucleosomal (147-294 base pairs) to nucleosome-free (<147 base pairs) fragments. Additionally, outlier cells were removed after scoring for the ratio of fragments centered at transcriptional start sites and the ratio of fragments in blacklisted regions, as defined by the ENCODE project. After filtering each sample for both RNA and ATAC data quality, the genomic coordinates of overlapping peaks from each individual sample were merged to define a common ATAC peak set for peak quantification across samples.

Transcriptomic data were normalized via SCTransform in Seurat, with regression of cell cycle genes (Seurat's *cc.genes*). ATAC data were normalized via term-frequency inverse-document-frequency (TF-IDF), and dimensional reduction was performed on the TF-IDF matrix via singular value decomposition (SVD), as part of the standard Signac workflow. Batch-correction was performed on both the RNA and ATAC modalities via the Harmony[49] package, and a multi-modal UMAP embedding was generated through the weighted-nearest neighbor (WNN) method with the FindMultiModalNeighbors function in Seurat. Clusters were identified on the WNN UMAP using the FindClusters function with algorithm 3 and cluster resolution 1.2.

Single-cell OCR Profiles & Motif Analysis

The model-based analysis of ChIP-seq (MACS2)[50] package was used to identify peaks within open chromatin regions. For comparisons of peak profiles, peaks present in at least 10% of the cells within the cluster were considered open in that cluster. Assessment of differential open chromatin accessibility was done with the FindMarkers function in Seurat to identify peaks present in 10% of cells with a log2 fold-change threshold of 0.5. Bonferroi-adjusted *p*-values were used to determine significance at an FDR < 0.05. Transcription factor activity was inferred via the chromVAR package[51] using the JASPAR2020[52] database. Differential transcription factor motif activity was calculated with the FindMarkers function at an FDR < 0.05.

Statistics

Statistical analyses were performed with the GraphPad Prism 9 software. Specific statistical tests were conducted as indicated in the figure legends.

Table S1. List of Antibodies for Flow Cytometry

Antibodies for Treg Isolation (FACS)				
staining reagent	conjugate	clone	vendor	cat no.
anti-CD4	FITC	RPA-T4	Biolegend	300538
anti-CD25	APC	4E3	ThermoFisher	17-0257-42
anti-CD127	PE	hIL-7R-M21	BD Biosciences	557938
Antibodies and reagents for Analytical Flow Cytometry				
staining reagent	conjugate	clone	vendor	
Fixable Live/Dead Viability Dye	eFluor780		eBioscience	65-0865
Fixable Viability Dye	Zombie UV		Biolegend	423108
anti-CD25	AF700	BC96	Biolegend	302622
anti-CD25	BV711	2A3	BD Biosciences	563159
anti-ICOS	PE-Cy7	C398.4a	Biolegend	313520
anti-ICOS	BUV805	DX29	BD Biosciences	748903
anti-TIGIT	PerCP-eFluor710	MBSA43	ThermoFisher	46-9500-42
anti-TIGIT	BV605	15153G	Biolegend	372712
anti-CD226	BV785	11A8	Biolegend	338322
anti-CD27	BV510	M-271	Biolegend	302836
anti-FOXP3	AF647	206D	Biolegend	320114
anti-HELIOS	FITC	22F6	Biolegend	137214
anti-HELIOS	PE-Cy7	22F6	Biolegend	137236
anti-CTLA4	PE	14D3	ThermoFisher	12-1529-42
anti-CTLA4	BUV737	14D3	ThermoFisher	367-1529-42
anti-CD40LG	BV421	24-31	Biolegend	310824
anti-IRF4	AF700	3E4	ThermoFisher	56-9858-82
anti-KI-67	BUV563	SolA15	ThermoFisher	365-5698-82
anti-IL-17A	PE	BL168	Biolegend	512306
anti-IFNg	BV785	4S.B3	Biolegend	502542
anti-IL-4	BV421	MP4-25D2	Biolegend	500826
anti-TNFa	FITC	Mab11	Biolegend	502906

Data Availability

The scMulti-omic data described in this manuscript have been deposited in the National Center for Biotechnology Information (NCBI) Gene Expression Omnibus (GEO) database (accession number is GSE281099).

Code Availability

The single-cell multi-omic (scATAC-seq and scRNA-seq) data analyses were performed using open-source algorithms as described in the Methods. Further details will be made available by the authors upon request.

References

1. Raffin, C., Vo, L. T. & Bluestone, J. A. Treg cell-based therapies: challenges and perspectives. *Nature Reviews Immunology* **20,** 158–172; 10.1038/s41577-019-0232-6 (2019).

2. Josefowicz, S. Z., Lu, L.-F. & Rudensky, A. Y. Regulatory T Cells: Mechanisms of Differentiation and Function. *Annual Review of Immunology* **30,** 531–564; 10.1146/annurev.immunol.25.022106.141623 (2012).

3. Sakaguchi, S., Sakaguchi, N., Asano, M., Itoh, M. & Toda, M. Immunologic self-tolerance maintained by activated T cells expressing IL-2 receptor alpha-chains (CD25). Breakdown of a single mechanism of self-tolerance causes various autoimmune diseases. *The Journal of Immunology* **155,** 1151–1164; 10.4049/jimmunol.155.3.1151 (1995).

4. Fontenot, J. D., Gavin, M. A. & Rudensky, A. Y. Foxp3 programs the development and function of CD4+CD25+ regulatory T cells. *Nature Immunology* **4,** 330–336; 10.1038/ni904 (2003).

5. Bennett, C. L. *et al.* The immune dysregulation, polyendocrinopathy, enteropathy, X-linked syndrome (IPEX) is caused by mutations of FOXP3. *Nature Genetics* **27,** 20–21; 10.1038/83713 (2001).

6. Bluestone, J. A. & Tang, Q. T_{reg} cells—the next frontier of cell therapy. *Science* **362,** 154–155; 10.1126/science.aau2688 (2018).

7. Selck, C. & Dominguez-Villar, M. Antigen-Specific Regulatory T Cell Therapy in Autoimmune Diseases and Transplantation. *Frontiers in Immunology* **12,** 661875; 10.3389/fimmu.2021.661875 (2021).

8. Tuomela, K., Salim, K. & Levings, M. K. Eras of designer Tregs: Harnessing synthetic biology for immune suppression. *Immunological reviews* **320,** 250–267; 10.1111/imr.13254 (2023).

9. Bluestone, J. A. *et al.* Type 1 diabetes immunotherapy using polyclonal regulatory T cells. *Science translational medicine* **7,** 315ra189; 10.1126/scitranslmed.aad4134 (2015).

10. Dall'Era, M. *et al.* Adoptive Treg Cell Therapy in a Patient With Systemic Lupus Erythematosus. *Arthritis & rheumatology (Hoboken, N.J.)* **71,** 431–440; 10.1002/art.40737 (2019).

11. Marek-Trzonkowska, N., Myśliwec, M., Siebert, J. & Trzonkowski, P. Clinical application of regulatory T cells in type 1 diabetes. *Pediatric Diabetes* **14,** 322–332; 10.1111/pedi.12029 (2013).

12. Sawitzki, B. *et al.* Regulatory cell therapy in kidney transplantation (The ONE Study): a harmonised design and analysis of seven non-randomised, single-arm, phase 1/2A trials. *Lancet (London, England)* **395,** 1627–1639; 10.1016/S0140-6736(20)30167-7 (2020).

13. Ho, P. *et al.* Harnessing regulatory T cells to establish immune tolerance. *Science translational medicine* **16,** eadm8859; 10.1126/scitranslmed.adm8859 (2024).

14. Zhou, X. *et al.* Instability of the transcription factor Foxp3 leads to the generation of pathogenic memory T cells in vivo. *Nature Immunology* **10,** 1000–1007; 10.1038/ni.1774 (2009).

15. Bailey-Bucktrout, S. L. *et al.* Self-antigen-Driven Activation Induces Instability of Regulatory T Cells during an Inflammatory Autoimmune Response. *Immunity* **39,** 949–962; 10.1016/j.immuni.2013.10.016 (2013).

16. Freuchet, A. *et al.* Identification of human exTreg cells as CD16+CD56+ cytotoxic CD4+ T cells. *Nature Immunology* **24,** 1748–1761; 10.1038/s41590-023-01589-9 (2023).

17. Miyara, M. *et al.* Functional Delineation and Differentiation Dynamics of Human CD4+ T Cells Expressing the FoxP3 Transcription Factor. *Immunity* **30,** 899–911; 10.1016/j.immuni.2009.03.019 (2009).

18. Hoffmann, P. *et al.* Loss of FOXP3 expression in natural human $CD4^{+}CD25^{+}$ regulatory T cells upon repetitive *in vitro* stimulation. *European Journal of Immunology* **39,** 1088–1097; 10.1002/eji.200838904 (2009).

19. Ohkura, N. *et al.* T Cell Receptor Stimulation-Induced Epigenetic Changes and Foxp3 Expression Are Independent and Complementary Events Required for Treg Cell Development. *Immunity* **37,** 785–799; 10.1016/j.immuni.2012.09.010 (2012).

20. Joudi, A. M., Reyes Flores, C. P. & Singer, B. D. Epigenetic Control of Regulatory T Cell Stability and Function: Implications for Translation. *Frontiers in Immunology* **13,** 861607; 10.3389/fimmu.2022.861607 (2022).

21. Samstein, R. M. *et al.* Foxp3 exploits a pre-existent enhancer landscape for regulatory T cell lineage specification. *Cell* **151,** 153–166; 10.1016/j.cell.2012.06.053 (2012).

22. Feng, Y. *et al.* Control of the Inheritance of Regulatory T Cell Identity by a cis Element in the Foxp3 Locus. *Cell* **158,** 749–763; 10.1016/j.cell.2014.07.031 (2014).

23. Trujillo-Ochoa, J. L., Kazemian, M. & Afzali, B. The role of transcription factors in shaping regulatory T cell identity. *Nature reviews. Immunology* **23,** 842–856; 10.1038/s41577-023-00893-7 (2023).

24. Delacher, M. *et al.* Transcriptional control of regulatory T cells. *Current topics in microbiology and immunology* **381,** 83–124; 10.1007/82_2014_373 (2014).

25. Fu, W. *et al.* A multiple redundant genetic switch locks in the transcriptional signature of T regulatory cells. *Nature Immunology* **13,** 972–980; 10.1038/ni.2420 (2012).

26. Schumann, K. *et al.* Functional CRISPR dissection of gene networks controlling human regulatory T cell identity. *Nature Immunology* **21,** 1456–1466; 10.1038/s41590-020-0784-4 (2020).

27. Morina, L. *et al.* Co-expression of Foxp3 and Helios facilitates the identification of human T regulatory cells in health and disease. *Frontiers in Immunology* **14,** 1114780; 10.3389/fimmu.2023.1114780 (2023).

555 28. Lam, A. J., Uday, P., Gillies, J. K. & Levings, M. K. Helios is a marker, not a driver, of
556 human Treg stability. *European Journal of Immunology* **52,** 75–84; 10.1002/eji.202149318
557 (2022).

558 29. Thornton, A. M. *et al.* Helios+ and Helios- Treg subpopulations are phenotypically and
559 functionally distinct and express dissimilar TCR repertoires. *European Journal of Immunology*
560 **49,** 398–412; 10.1002/eji.201847935 (2019).

561 30. Takatori, H. *et al.* Helios Enhances Treg Cell Function in Cooperation With FoxP3.
562 *Arthritis & rheumatology (Hoboken, N.J.)* **67,** 1491–1502; 10.1002/art.39091 (2015).

563 31. Herppich, S. *et al.* Dynamic Imprinting of the Treg Cell-Specific Epigenetic Signature in
564 Developing Thymic Regulatory T Cells. *Frontiers in Immunology* **10,** 2382;
565 10.3389/fimmu.2019.02382 (2019).

566 32. Zheng, Y. *et al.* Role of conserved non-coding DNA elements in the Foxp3 gene in
567 regulatory T-cell fate. *Nature* **463,** 808–812; 10.1038/nature08750 (2010).

568 33. Brown, M. E. *et al.* Human CD4+CD25+CD226- Tregs Demonstrate Increased Purity,
569 Lineage Stability, and Suppressive Capacity Versus CD4+CD25+CD127lo/- Tregs for Adoptive
570 Cell Therapy. *Frontiers in Immunology* **13,** 873560; 10.3389/fimmu.2022.873560 (2022).

571 34. Nowak, A. *et al.* CD137+CD154- Expression As a Regulatory T Cell (Treg)-Specific
572 Activation Signature for Identification and Sorting of Stable Human Tregs from In Vitro
573 Expansion Cultures. *Frontiers in Immunology* **9,** 199; 10.3389/fimmu.2018.00199 (2018).

574 35. Zheng, Y. *et al.* Regulatory T-cell suppressor program co-opts transcription factor IRF4 to
575 control T(H)2 responses. *Nature* **458,** 351–356; 10.1038/nature07674 (2009).

576 36. Glasmacher, E. *et al.* A genomic regulatory element that directs assembly and function
577 of immune-specific AP-1-IRF complexes. *Science (New York, N.Y.)* **338,** 975–980;
578 10.1126/science.1228309 (2012).

579 37. Krishnamoorthy, V. *et al.* The IRF4 Gene Regulatory Module Functions as a Read-Write
580 Integrator to Dynamically Coordinate T Helper Cell Fate. *Immunity* **47,** 481-497.e7;
581 10.1016/j.immuni.2017.09.001 (2017).

582 38. Conley, J. M., Gallagher, M. P., Rao, A. & Berg, L. J. Activation of the Tec Kinase ITK
583 Controls Graded IRF4 Expression in Response to Variations in TCR Signal Strength. *Journal of*
584 *immunology (Baltimore, Md. : 1950)* **205,** 335–345; 10.4049/jimmunol.1900853 (2020).

585 39. Marson, A. *et al.* Foxp3 occupancy and regulation of key target genes during T-cell
586 stimulation. *Nature* **445,** 931–935; 10.1038/nature05478 (2007).

587 40. Miyao, T. *et al.* Plasticity of Foxp3(+) T cells reflects promiscuous Foxp3 expression in
588 conventional T cells but not reprogramming of regulatory T cells. *Immunity* **36,** 262–275;
589 10.1016/j.immuni.2011.12.012 (2012).

590 41. Sidwell, T. *et al.* Attenuation of TCR-induced transcription by Bach2 controls regulatory T
591 cell differentiation and homeostasis. *Nature communications* **11,** 252; 10.1038/s41467-019-
592 14112-2 (2020).

42. Arnold, P. R. *et al.* Suppression of FOXP3 expression by the AP-1 family transcription factor BATF3 requires partnering with IRF4. *Frontiers in Immunology* **13,** 966364; 10.3389/fimmu.2022.966364 (2022).

43. Man, K. *et al.* The transcription factor IRF4 is essential for TCR affinity-mediated metabolic programming and clonal expansion of T cells. *Nature Immunology* **14,** 1155–1165; 10.1038/ni.2710 (2013).

44. Bagadia, P. *et al.* An Nfil3-Zeb2-Id2 pathway imposes Irf8 enhancer switching during cDC1 development. *Nature Immunology* **20,** 1174–1185; 10.1038/s41590-019-0449-3 (2019).

45. Ohkura, N. & Sakaguchi, S. Transcriptional and epigenetic basis of Treg cell development and function: its genetic anomalies or variations in autoimmune diseases. *Cell Research* **30,** 465–474; 10.1038/s41422-020-0324-7 (2020).

46. Hao, Y. *et al.* Integrated analysis of multimodal single-cell data. *Cell* **184,** 3573-3587.e29; 10.1016/j.cell.2021.04.048 (2021).

47. Stuart, T., Srivastava, A., Madad, S., Lareau, C. A. & Satija, R. Single-cell chromatin state analysis with Signac. *Nature methods* **18,** 1333–1341; 10.1038/s41592-021-01282-5 (2021).

48. Young, M. D. & Behjati, S. SoupX removes ambient RNA contamination from droplet-based single-cell RNA sequencing data. *GigaScience* **9**; 10.1093/gigascience/giaa151 (2020).

49. Korsunsky, I. *et al.* Fast, sensitive and accurate integration of single-cell data with Harmony. *Nature methods* **16,** 1289–1296; 10.1038/s41592-019-0619-0 (2019).

50. Zhang, Y. *et al.* Model-based analysis of ChIP-Seq (MACS). *Genome biology* **9,** R137; 10.1186/gb-2008-9-9-r137 (2008).

51. Schep, A. N., Wu, B., Buenrostro, J. D. & Greenleaf, W. J. chromVAR: inferring transcription-factor-associated accessibility from single-cell epigenomic data. *Nature methods* **14,** 975–978; 10.1038/nmeth.4401 (2017).

52. Fornes, O. *et al.* JASPAR 2020: update of the open-access database of transcription factor binding profiles. *Nucleic acids research* **48,** D87-D92; 10.1093/nar/gkz1001 (2020).

Acknowledgement
The authors would like to thank Vinh Nguyen, Charlotte Monsour, Yue Chen, and the UCSF Parnassus Flow Cytometry CoLab (PFCC) for technical support. We also thank Alexander Marson, Jennifer Umhoefer, Frederic van Gool, and Joe Arron for insightful discussion and critical feedback. This work was funded in part by grants from NIH (UC4 DK116264 to J.A.B., Q.T.), Leona M. and Harry B. Helmsley Charitable Trust (G-2109-04813 to Q.T.), Sonoma Biotherapeutics (Q.T.), Breakthrough T1D (COE-2019-860-S-B, to Q.T.), and an NIH postdoctoral fellowship (T32 5T32AI007334-35 to P.H.)

Author Information

Patrick Ho
Current address: Medizinische Klinik und Poliklinik II, Universitätsklinikum Würzburg, 97080 Würzburg, Germany

Jeffrey A. Bluestone
Current address: Sonoma Biotherapeutics, South San Francisco, CA 94080

Authors and affiliations

Diabetes Center, University of California, San Francisco, San Francisco, CA, USA
Patrick Ho, Wendy, Rosenthal, Jeffrey A. Bluestone, Qizhi Tang

Department of Surgery, University of California, San Francisco, San Francisco, CA USA
Qizhi Tang

Gladstone-UCSF Institute of Genomic Immunology, San Francisco, San Francisco, CA, USA
Qizhi Tang

Contributions
P.H., J.A.B., and Q.T. conceived and designed the study. P.H. and W.R. performed the experiments. P.H. and Q.T. analyzed the data. P.H. wrote the original draft, and P.H., J.A.B., and Q.T. reviewed and edited the manuscript.

*Corresponding author
Correspondence to qizhi.tang@ucsf.edu

Ethics declarations
P.H. has no financial interests to report. P.H. is a coinventor of the following relevant pending patent: US Patent Application No. 63/571,413. W.R. has no conflict to report. Q.T. is a cofounder and shareholder of Sonoma Biotherapeutics, holds shares of stock in eGenesis, and is a scientific advisor for Sonoma Biotherapeutics, Qihan Bio, Minutia, Moderna, and Waypoint Bio. Q.T. is a coinventor of the following relevant issued patents and pending patents: US9801911B2, US7722862B2, PCT/US2019/022546, PCT/US2019/023883, PCT/US2020/030869, PCT/US2021/072139, PCT/US2021/049682, PCT/US2022/074720, and US Patent Application No. 63/571,413. J.A.B. is CEO and president and has a financial interest in Sonoma Biotherapeutics and is on the board of directors and has financial interests in Gilead. J.A.B. is a coinventor of the following relevant issued patents and pending patents: PCT/US20230280341A1, PCT/US9801911B2, aU2016211161C1, PCT/US10138298B2,

PCT/US7722862B2, PCT/US2019/022546, PCT/US2019/023883, PCT/US2021/072139, PCT/US2021/049682, and US Patent Application No. 63/571,413.

Figures

Figure 1

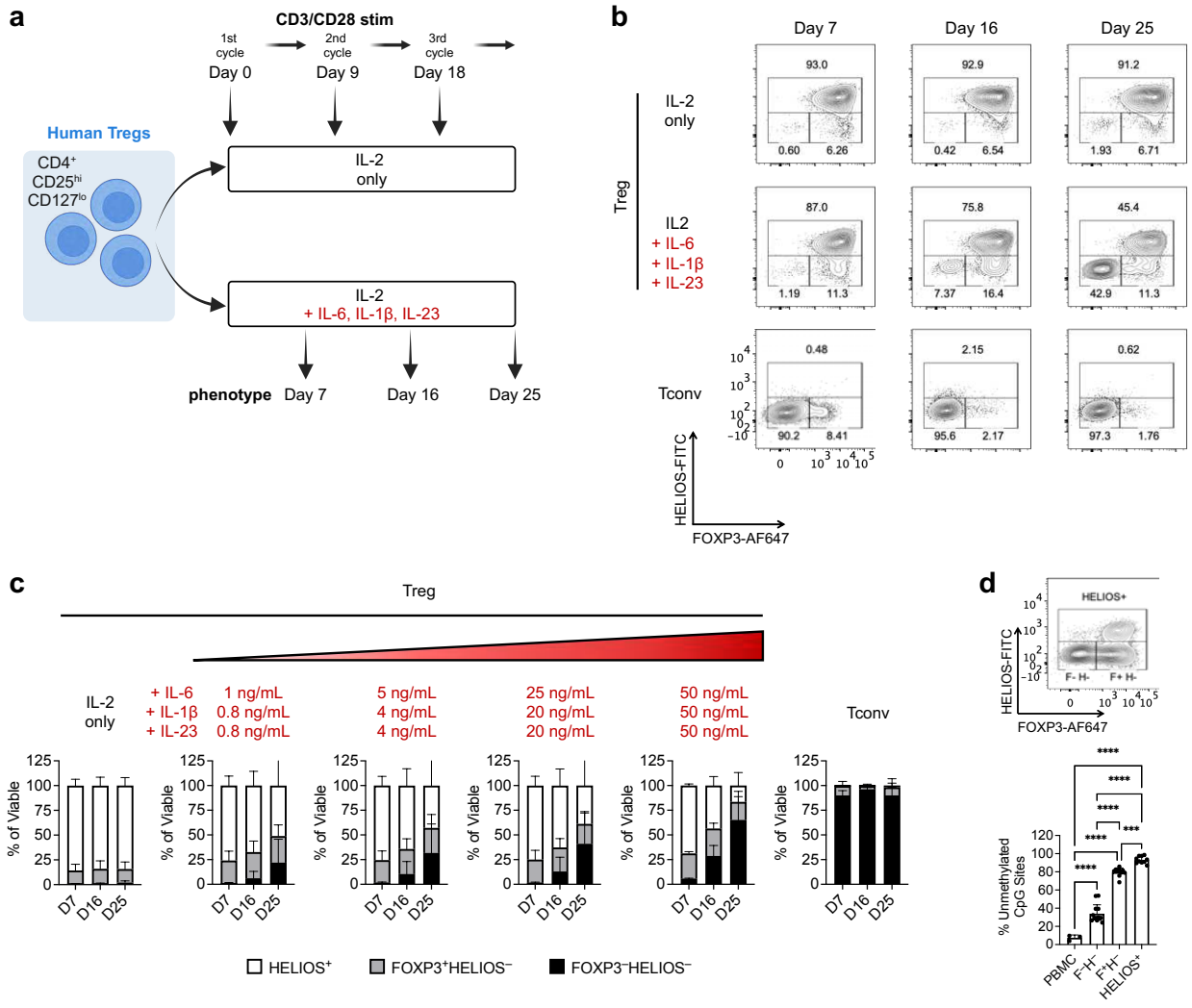


Figure 1. Primary human Tregs undergo progressive destabilization during repeated *in vitro* CD3/CD28 stimulation under sustained inflammatory cytokine exposure. (a) Primary human $CD4^+CD25^+CD127^{lo/-}$ Tregs were stimulated with anti-CD3/CD28 every 9 days in the presence or absence of IL-6, IL-1β, IL-23. Expression of FOXP3 and HELIOS was assessed at day 7 of each stimulation cycle via flow cytometry. **(b)** Representative FOXP3 and HELIOS flow cytometry profiles at days 7, 16, and 25. Labels indicate the percentage of cells in the gated sub-populations for $HELIOS^+$ (top), $FOXP3^+HELIOS^-$ (bottom right), and $FOXP3^-HELIOS^-$ (bottom left). Profiles of $CD4^+$ conventional T cells (Tconvs) are shown for comparison. **(c)** Tregs were cultured as in (A) and challenged with the triple combination of IL-6, IL-1β, and IL-23 across a 50-fold concentration range. Average distribution of cells within each gated sub-population from (B) at days 7, 16, and 25 is summarized. Results are a summary of data using Tregs from 5-8 unrelated normal donors. **(d)** Percentage of unmethylated CpG sites at the *FOXP3* CNS2 (TSDR) from each of the FACS-purified HELIOS+, $FOXP3^+HELIOS^-$ (F^+H^-), or $FOXP3^-HELIOS^-$ (F^-H^-) sub-populations, as determined by pyrosequencing of bisulfite-

689 converted genomic DNA. Results in panels (c) and (d) are shown as mean ± standard
690 deviations. Statistical significance was calculated via one-way ANOVA with post Tukey test, ***
691 p < 1e-3, ****p < 1e-4.

Figure 2

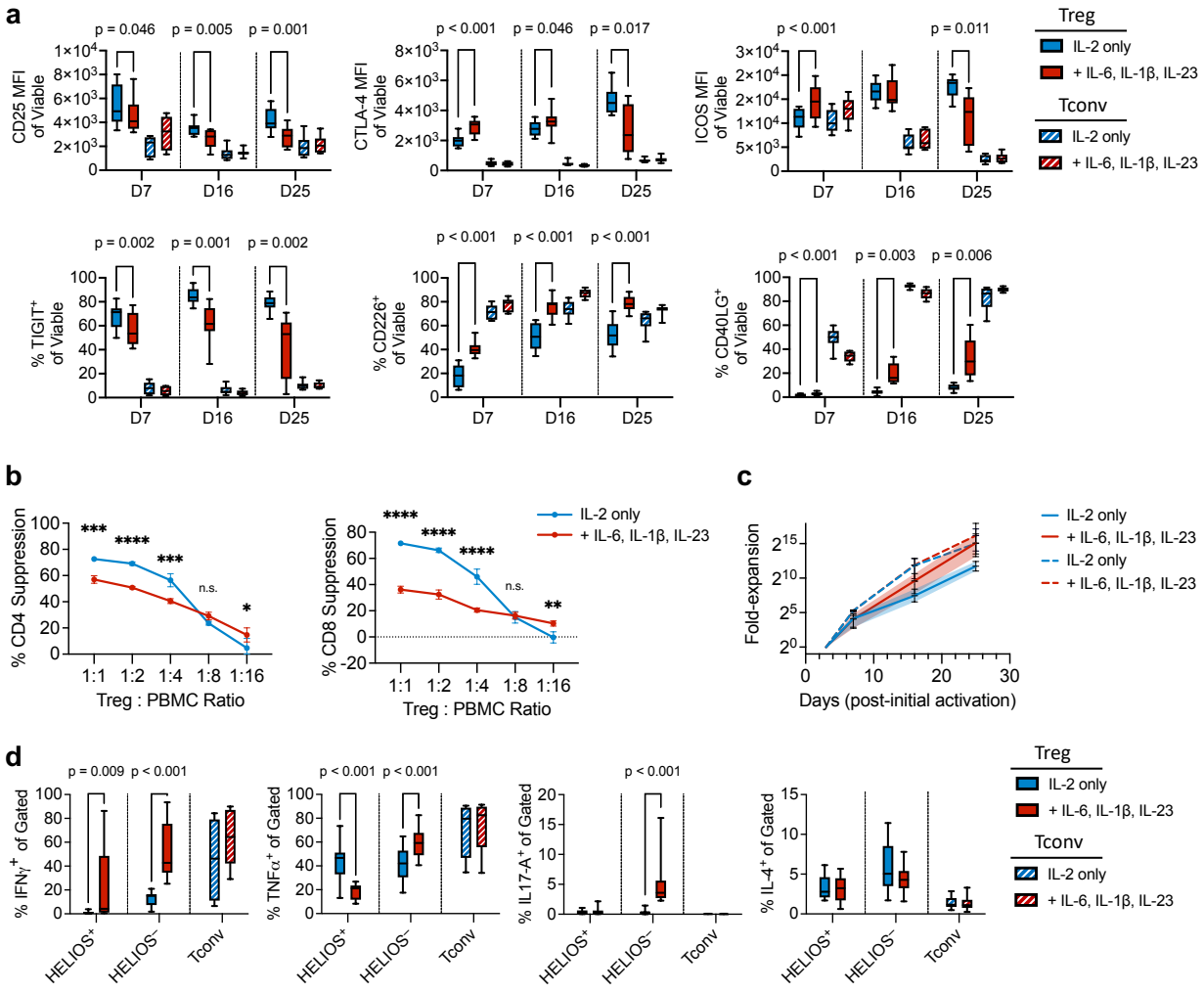


Figure 2. Inflammatory cytokine-induced reprogramming results in human Treg dysfunction. (a) The expression of common phenotypic markers was assessed via flow cytometry at days 7, 16, and 25 for primary human Tregs and Tconvs cultured in IL-2 alone or in the added presence of IL-6, IL-1β, and IL-23. Average geometric mean of fluorescence intensity (MFI; CD25, CTLA-4, ICOS) or percent positive (TIGIT, CD226, CD40LG) of common Treg phenotypic markers is summarized. Bars represent the inner quartile ranges, lines inside the bars represent medians, and the whiskers represent ranges from minimum to maximum. **(b)** After 25 days of *in vitro* culture, Tregs were co-cultured with PBMCs at the indicated Treg:PBMC ratios. *In vitro* suppression of responder $CD4^+$ (left) and $CD8^+$ (right) T-cell proliferation relative to proliferation of the respective responder population in PBMC-only samples. Results are shown as mean ± standard deviations. Statistical significance was calculated via two-way ANOVA with post hoc Tukey test. n.s. = not significant, *p < 5e-2, *p < 5e-3, ***p < 5e-4, ****p < 1e-4. **(c)** Cumulative fold-expansion of Tregs and Tconvs over 25 days of *in vitro* culture in the presence or absence of IL-6, IL-1β, and IL-23. Results are shown as mean (lines) ± standard deviations (shaded regions). **(d)** At day 25, cells were stimulated for 5 h with PMA and ionomycin and the expression of pro-inflammatory cytokines was assessed via intracellular flow staining. Percentage of cells expressing IFNγ, TNFα, IL-17A, and IL-4 amongst expanded $HELIOS^+$ Tregs, $HELIOS^-$ Tregs, and Tconvs is summarized. Bars represent the inner quartile

ranges, lines inside the bars represent medians, and the whiskers represent ranges from minimum to maximum. Data in (a, c-d) are from n = 8 normal human donors. Statistical significance in (a) and (d) were calculated via paired t tests.

Figure 3

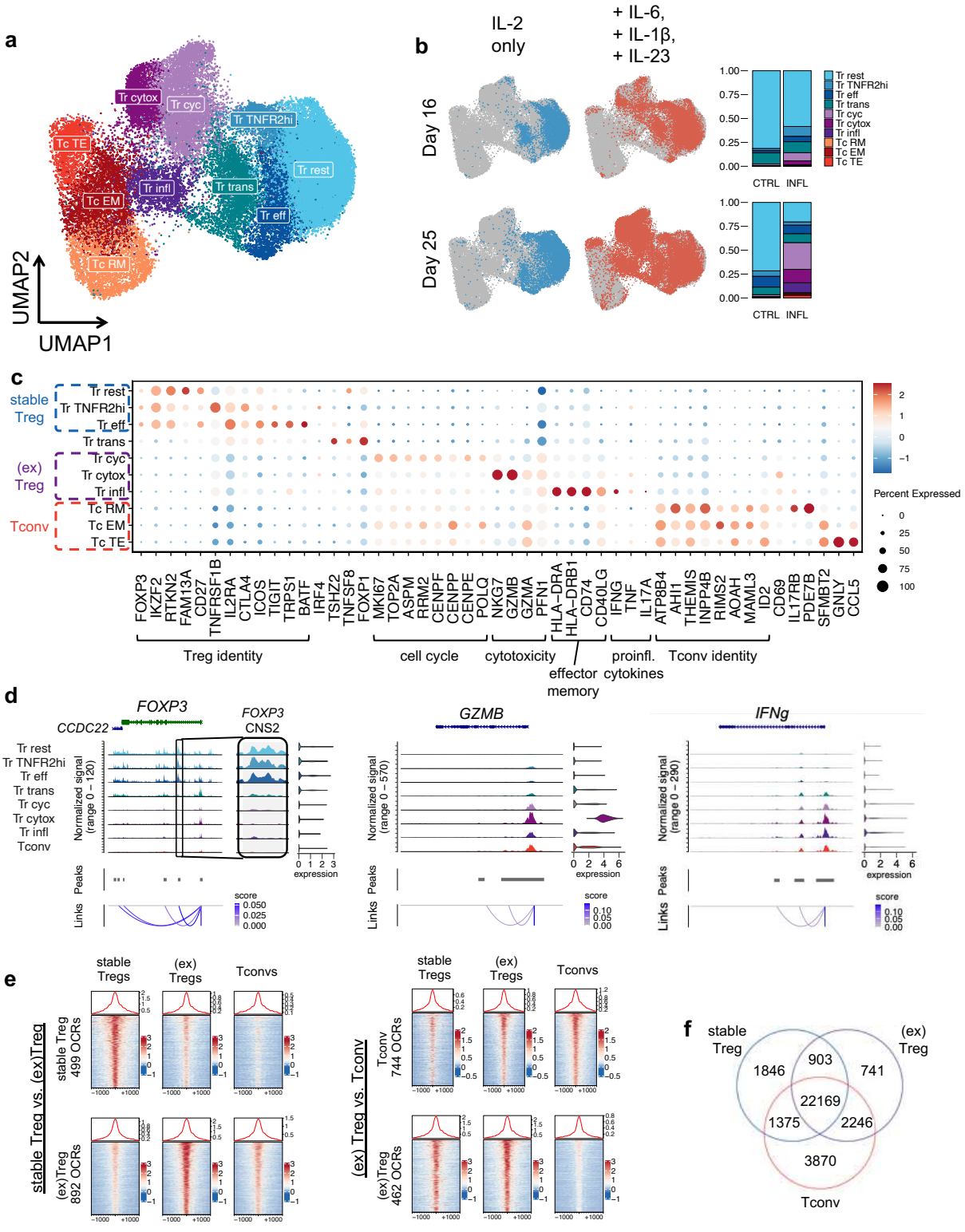


Figure 3. Single-cell multi-omic profiles of gene expression and chromatin accessibility reveal molecular hallmarks of Treg lineage-decommitment. (a) Single-cell multi-omic profiles were generated from Tregs and Tconvs isolated from 3 unrelated normal human donors.

The cells were stimulated and cultured in the presence or absence of IL-6, IL-1β, and IL-23 as described in Figure 1A. Cells were harvested on days 16 and 25 of culture for single-cell multi-omic analysis. Unsupervised clustering on a weighted nearest neighbor (WNN) UMAP resulted in the identification of 10 cell clusters shown in distinct colors. **(b)** Cluster distributions for day 16 and day 25 samples from Tregs expanded in IL-2 only or IL-2 plus IL-6, IL-1β, and IL-23. **(c)** Transcriptional signatures of cell clusters identified in (A) are shown, with additional annotations to group phenotypically suppressive (stable) Tregs, destabilized (ex)Tregs, and Tconvs. **(d)** Pseudobulk chromatin accessibility tracks and corresponding gene expression violin plots are shown for each cluster at the *FOXP3* (CNS2 highlighted), *IFNG*, and *GZMB* loci. ATAC-seq–defined OCRs (peaks) and correlations between peaks and transcript expression (links) are shown for each locus. **(e)** Heat maps of chromatin accessibility for stable Tregs, (ex)Tregs, and Tconvs at open chromatin regions (OCRs) identified as differentially accessible between the indicated cell states. **(f)** Venn diagram of shared and unique OCRs in stable Tregs, (ex)Tregs, and Tconvs.

Figure 4

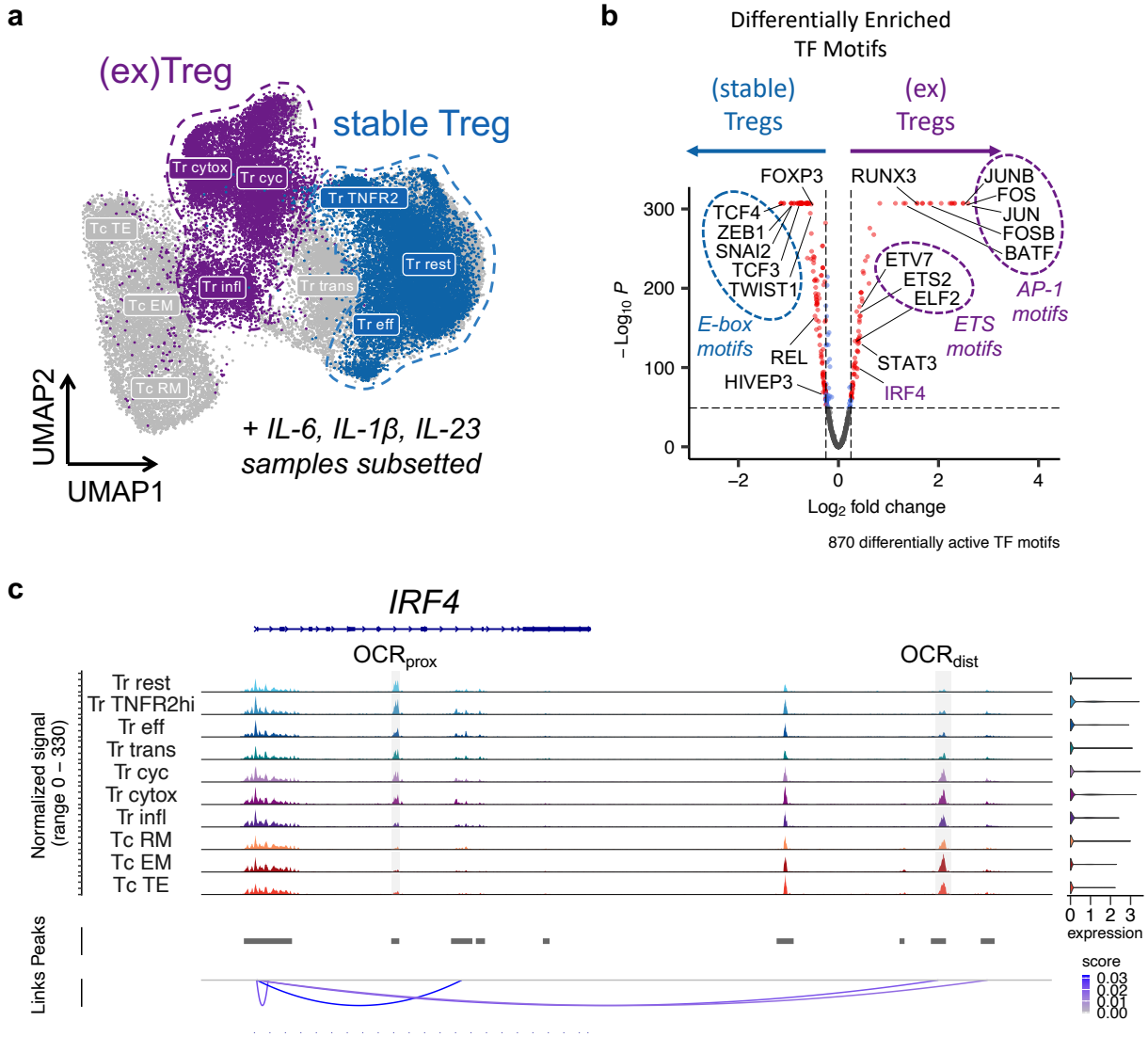
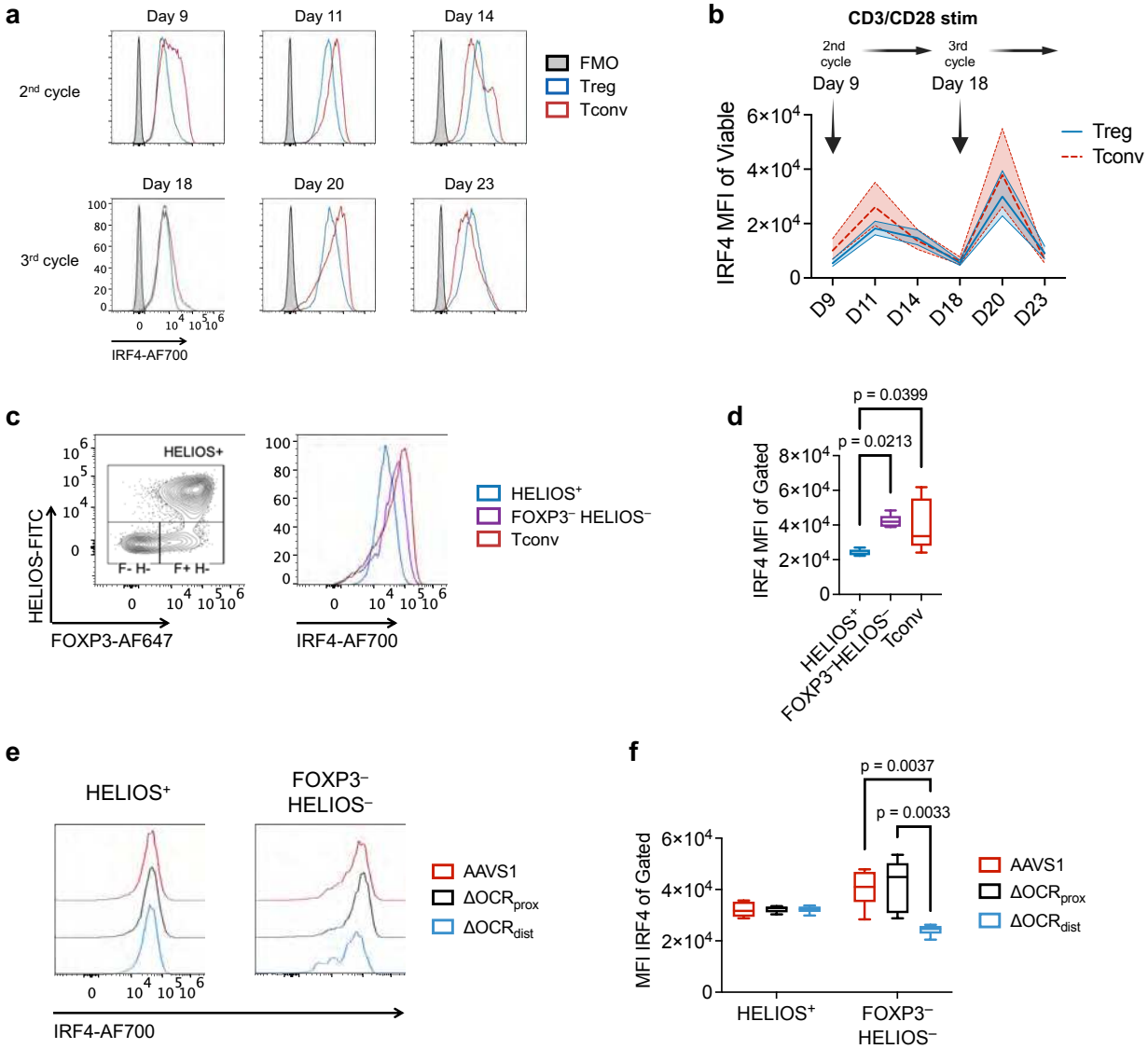


Figure 4. Tregs undergo a reciprocal switch in chromatin accessibility at the *IRF4* locus. **(a)** TF motif enrichment analysis was performed on stable Treg and (ex)Treg clusters from IL-6, IL-1β, and IL-23 treated samples to identify putative drivers of Treg destabilization. **(b)** Volcano plot of differentially enriched TF motifs in stable Tregs and destabilized Tregs, with the E-box, AP-1, and ETS TF families highlighted. **(c)** Pseudobulk chromatin accessibility tracks and corresponding gene expression violin plots for the *IRF4* locus. The peak linkages (blue lines, bottom) indicate regions that coordinately influence gene expression. The OCR_{prox} and OCR_{dist} regions are highlighted in the shaded regions.

Figure 5



738 **Figure 5. OCR_{dist} selectively promotes TCR-triggered IRF4 upregulation in destabilized**
739 **$FOXP3^{-}HELIOS^{-}$ Tregs. (a)** Primary human Tregs and Tconvs were expanded in the presence
740 of IL-6, IL-1β, and IL-23 and re-stimulated with anti-CD3/CD28 every 9 days. Flow cytometry
741 histograms for IRF4 expression in each cell type at 0, 2, and 5 days of each restimulation cycle.
742 **(b)** Geometric mean fluorescence intensity for IRF4 expression in Tregs and Tconvs (n = 5
743 normal human donors) with average and standard error of mean indicated by the lines and
744 shaded regions, respectively. **(c)** Representative HELIOS vs. FOXP3 profile and histogram of
745 IRF4 expression for $HELIOS^{+}$ (stable) Tregs, $FOXP3^{-}HELIOS^{-}$ (destabilized) Tregs, and Tconvs
746 at day 25 of culture with IL-6, IL-1β, and IL-23. **(d)** Geometric mean fluorescence intensity of
747 IRF4 expression (n = 5 normal human donors) for the samples in (c) is summarized. **(e)**
748 CRISPR/Cas9 ribonucleoprotein complexes were delivered via electroporation to excise
749 OCR_{prox} and OCR_{dist} prior to inflammatory cytokine exposure with IL-6, IL-1β, and IL-23.
750 Representative histograms for IRF4 expression in $HELIOS^{+}$ (stable) and $FOXP3^{-}$ $HELIOS^{-}$
751 (destabilized) sub-populations from AAVS1-edited, ΔOCR_{prox}, and ΔOCR_{dist} Tregs at Day 20 of
752 *in vitro* culture. **(f)** Geometric mean fluorescence intensity of IRF4 expression (n = 6 normal

753 human donors) for the samples in (e) is summarized. Statistical significance was calculated via
754 one-way ANOVA with post Tukey test.

Figure 6

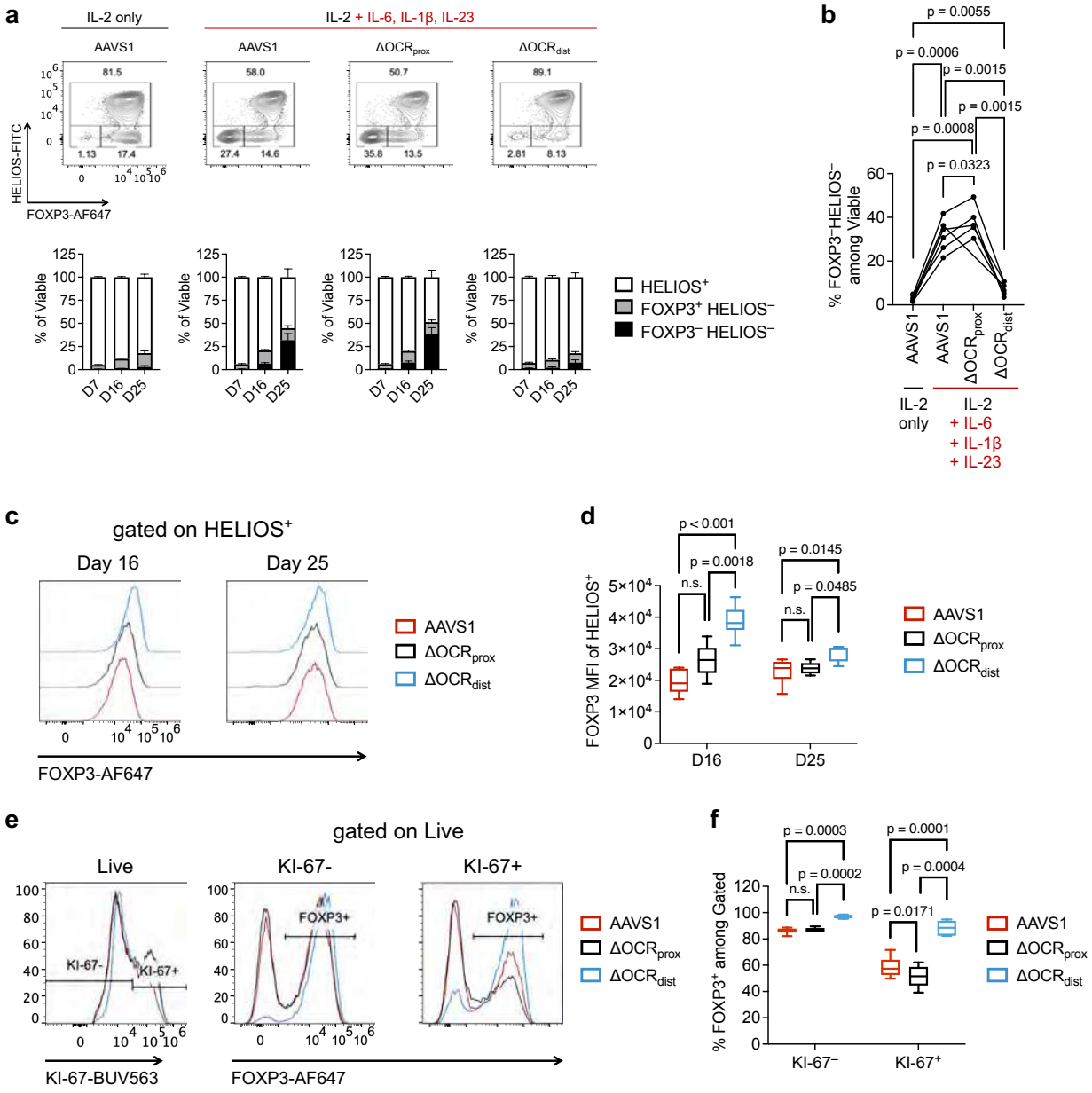


Figure 6. Non-coding *IRF4* regulatory elements modulate Treg stability during inflammatory cytokine exposure. (a) Primary human Tregs were electroporated with CRISPR/Cas9 ribonucleoproteins (RNPs) designed to target AAVS1 or to excise either OCR_{prox} or OCR_{dist}. Tregs were subsequently challenged with repeated anti-CD3/CD28 stimulation and sustained IL-6, IL-1β, and IL-23 exposure to induce destabilization. Representative expression profiles for FOXP3 and HELIOS (top) and the summarized average distribution amongst $HELIOS^+$, $FOXP3^+HELIOS^-$, and $FOXP3^-HELIOS^-$ populations (bottom) at day 25 are shown. **(b)** Donor-matched comparison of the fraction of viable cells that converted into $FOXP3^-HELIOS^-$ cells by day 25 is summarized. **(c)** Representative histograms of FOXP3 expression amongst the $HELIOS^+$ (stable) population from AAVS1-edited, ΔOCR_{prox}, and ΔOCR_{dist} Tregs at days 16 and 25 of culture with IL-6, IL-1β, and IL-23 exposure are shown. **(d)** Geometric mean

fluorescence intensity of FOXP3 expression in HELIOS$^+$ Tregs for the samples in (c). **(e)** Representative histograms and gating for KI-67 expression amongst all live cells (left) and FOXP3 expression amongst live KI-67$^-$ (middle) or KI-67$^+$ cells (right). **(f)** Percentage of FOXP3-expressing cells amongst KI-67$^-$ (non-proliferating) and KI-67$^+$ (proliferating) cells 7 days (day 25) after restimulation on day 18. Data are from n = 5-6 normal human donors. Statistical significance was calculated via one-way ANOVA with post Tukey test.

Figure 7

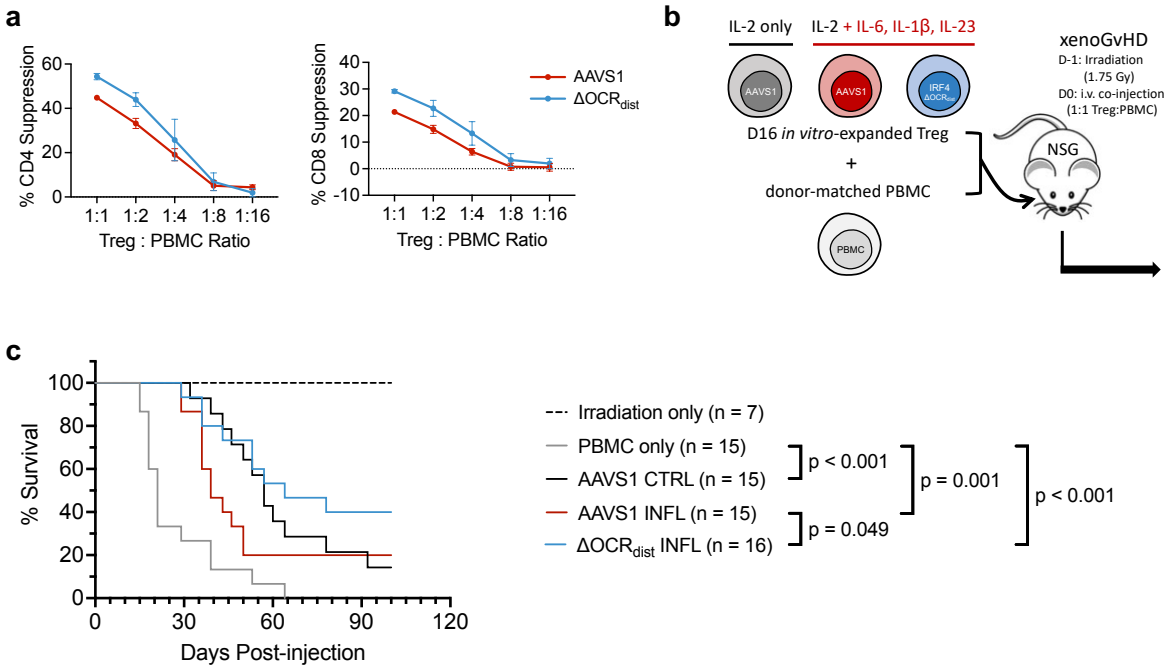


Figure 7. ΔOCR$_{dist}$ Tregs exhibit greater *in vitro* suppressive activity and mediate greater protection from xenogeneic graft-versus-host disease. (a) AAVS1 and ΔOCR$_{dist}$ CRISPR-edited primary human Tregs were challenged with repeated anti-CD3/CD28 stimulation cycles under IL-6, IL-1β, and IL-23 exposure to induce destabilization. At day 25, the resulting cells were co-cultured with PBMCs at the specified Treg:PBMC ratios. Percent *in vitro* suppression of responder CD4$^+$ (left) and CD8$^+$ (right) T-cell proliferation relative to the respective responder populations in PBMC-only (no Treg) controls. **(b)** AAVS1 and ΔOCR$_{dist}$ CRISPR-edited primary human Tregs were expanded in the presence or absence of IL-6, IL-1β, and IL-23 for 16 days to sensitize the Tregs to inflammatory cytokine-induced instability. After 16 days of *in vitro* expansion, Tregs and donor-matched PBMCs were co-injected into pre-irradiated NSG mice at 1:1 Treg:PBMC ratio. Mice weighed twice weekly and monitored for signs of GvHD. **(c)** Survival curve for irradiation only (no cells injected), PBMC only (no Tregs), AAVS1-edited expanded in IL-2–only conditions (AAVS1 CTRL), and inflammatory cytokine-challenged AAVS1-edited (AAVS1 INFL) and ΔOCR$_{dist}$ (ΔOCR$_{dist}$ INFL) groups. Data are pooled from an experiment using 2 normal human donors. Statistical significance was determined via Gehan-Brewslow-Wilcoxon test.

Supplementary Files

This is a list of supplementary files associated with this preprint. Click to download.

- 241018SupplementvSubmit.pdf
- 241105SupplementvSubmitNIFormat.pdf